HHS Public Access

Author manuscript

Prostaglandins Other Lipid Mediat. Author manuscript; available in PMC 2022 June 01.

Published in final edited form as:

Prostaglandins Other Lipid Mediat. 2021 June ; 154: 106548. doi:10.1016/j.prostaglandins.2021.106548.

20-HETE-promoted cerebral blood flow autoregulation is associated with enhanced pericyte contractility

Yedan Liu[1,2,*], **Huawei Zhang**[2,*], **Celeste YC. Wu**[3], **Tina Yu**[2], **Xing Fang**[2], **Jane J. Ryu**[2], **Baoying Zheng**[2], **Zongbo Chen**[1], **Richard J. Roman**[2], **Fan Fan**[2,§]

[1]Department of Pediatrics, The Affiliated Hospital of Qingdao University, Qingdao, Shandong 266003, China

[2]Department of Pharmacology and Toxicology, University of Mississippi Medical Center, Jackson, Mississippi 39216, USA

[3]Department of Neurology, Louisiana State University Health Sciences Center, Shreveport, Louisiana 71130, USA

Abstract

We previously reported that deficiency in 20-HETE or CYP4A impaired the myogenic response and autoregulation of cerebral blood flow (CBF) in rats. The present study demonstrated that CYP4A was coexpressed with alpha-smooth muscle actin (α-SMA) in vascular smooth muscle cells (VSMCs) and most pericytes along parenchymal arteries (PAs) isolated from SD rats. Cell contractile capabilities of cerebral VSMCs and pericytes were reduced with a 20-HETE synthesis inhibitor, HET0016 but restored with 20-HETE analog WIT003. Similarly, intact myogenic responses of the middle cerebral artery and PA of SD rats decreased with HET0016 and were rescued by WIT003. The myogenic response of the PA was abolished in SS and was restored in SS.BN5 and SS. *Cyp4a1* rats. HET0016 enhanced CBF and impaired its autoregulation in the surface and deep cortex of SD rats. These results demonstrate that 20-HETE has a direct effect on cerebral mural cell contractility that may play an essential role in controlling cerebral vascular function.

Keywords

20-Hydroxyeicosatetraenoic acid; pericytes; vascular smooth muscle cells; cell contractility; myogenic response; cerebral blood flow autoregulation

§ Send Correspondence to: Fan Fan, M.D., M.S., FAHA, University of Mississippi Medical Center, Department of Pharmacology and Toxicology, 2500 North State Street, Jackson, MS 39216, Ph: 601-984-1553, Fax: 601-984-1637, ffan@umc.edu.

*Y. Liu and H. Zhang contributed equally to this work.

Declaration of competing interest

None.

1. Introduction

20-Hydroxyeicosatetraenoic acid (20-HETE) is an arachidonic acid metabolite by enzymes of CYP4A and CYP4F families. It has diverse physiological and pathological effects on cardiovascular function, suggesting it may play a role in the pathogenesis, progression, and prognosis of various cardiovascular diseases [1–9]. 20-HETE contributes to sodium transport regulation, endothelial dysfunction, vasoconstriction, inflammation, angiogenesis, vascular remodeling, and restenosis. Alteration of 20-HETE production has been linked to hypertension; stroke; Alzheimer's disease (AD); ischemia-reperfusion injury in the kidney, brain, and heart; as well as changes in airway and placenta vascular resistance [1, 10–14].

We have been studying the roles of 20-HETE in cerebral vascular function for decades. Our previous studies demonstrated that Dahl salt-sensitive (SS) rats have a genetic deficiency in the production of 20-HETE and the expression of CYP4A enzymes [15]. They exhibited impaired myogenic response of the middle cerebral artery (MCA) and autoregulation of cerebral blood flow (CBF) [16]. This impaired cerebral vascular hemodynamics found in SS rats is associated with enhanced blood-brain barrier (BBB) leakage in response to acute hypertension, which was rescued by transferring chromosome 5 containing the *Cyp4a1, 4a2, 4a3,* and *4a8* genes from Brown Norway (BN) and knocking in wildtype *Cyp4a1* onto the SS transgenic background [16]. On the other hand, previous studies demonstrated that inhibition of 20-HETE attenuated inflammation and oxidative stress in spontaneously hypertensive rats (SHR) in association with improvement of cerebral vascular function [9], and the enhanced cerebral vascular production of 20-HETE in this model was in association with ischemic stroke [17]. These results in terms of the role of 20-HETE and cerebral vascular function are controversial, possibly because different models with different genetic, anatomic, endocrine, and metabolic physiological or pathological conditions only display a "summarized" cerebral vascular phenotype. However, whether 20-HETE plays a direct role in cerebral vascular reactivity and the direction of its effect on the alternation of susceptibility to stroke and cognitive deficits have not been studied. In this regard, human studies demonstrated that genetic variants of *CYP4A11* and *CYP4F2,* the most potent enzymes producing 20-HETE in humans, have been linked to hypertension and stroke [18–29]. Several of these variants were validated *in vitro* that reduce the production of 20-HETE [24, 27, 30]. Furthermore, we previously reported that genetic variants in these two genes are associated with loss of cortical, hippocampal, and AD signature volumes and cognitive dysfunction in 4,286 elderly subjects in the Atherosclerosis Risk in Communities Neurocognitive Study (ARIC-NCS) [10].

20-HETE has been reported to be produced in cerebral vascular smooth muscle cells (VSMCs), endothelial cells (ECs), pericytes, astrocytes, neurons, and podocytes [31–36]. It has been well established that cerebral VSMCs play an essential role in the regulation of the myogenic response and autoregulation in the cerebral circulation [6, 37, 38]. More recently, emerging evidence indicated that cerebrovascular pericytes expressing alpha-smooth muscle actin (α-SMA) that primarily localize on precapillary arterioles also participate in controlling CBF and maintaining cerebral vascular function with their contractile capability [39–50]. However, whether 20-HETE directly constricts cerebrovascular pericytes and precapillary arterioles and whether it is related to CBF autoregulation in the deep brain

cortex have never been studied. The present study seeks to answer these questions using pharmaceutical intervention with a stable 20-HETE analog 20-hydroxyeicosa-5(Z),14(Z)-dienoic acid (WIT003), and a 20-HETE synthesis inhibitor N-Hydroxy-N′-(4-butyl-2-methylphenyl)-formamidine (HET0016) [51–53], as well as SS, SS.BN5 and SS.*Cyp4a1* rats since the production of 20-HETE in the cerebral vasculature was 6-fold higher in the latter two strains than SS rats [16]. We first identified the expression pattern of CYP4A in cerebral mural cells of the MCAs, penetrating arterioles, and parenchymal arterioles (PAs). We then examined the effects of 20-HETE on the contractile capability of α-SMA$^+$ cerebral pericytes and primary VSMCs isolated from the MCA of Sprague Dawley (SD) rats. We also studied the effects of 20-HETE on the myogenic response of the PAs and CBF autoregulation in the surface and deep cortex of these rats.

2. Materials and methods

2.1. Animals

All experiments were performed using male SD rats purchased from Envigo (Indianapolis, IN) and our in house colonies of SS, SS.BN5 and SS. *Cyp4a1* rats. All animals were housed following standard laboratory animal conditions, maintained with free access to food and water ad libitum. The University of Mississippi Medical Center (UMMC) animal care facility is approved by the American Association for the Accreditation of Laboratory Animal Care. The animal protocols were approved by the Institutional Animal Care and Use Committees (IACUC) of the UMMC and followed the NIH's relevant biosafety policy and guidance.

2.2. Cell culture

Primary cerebral VSMCs were isolated from the MCA of 3-week old male SD rats, as described earlier [54–57]. Briefly, the MCAs that were dissected from the brain were placed in ice-cold Tyrode's solution, containing 145 mM NaCl, 6 mM KCl, 1 mM $MgCl_2.6H_2O$, 50 uM $CaCl_2.2H_2O$, 10 mM HEPES sodium salt, 4.2 mM $NaHCO_3$, 10 mM Glucose; pH 7.4. After incubation with papain (22.5 u/mL) and dithiothreitol (2 mg/mL) in the Tyrode's solution at 37 °C for 15 minutes, the MCAs were centrifuged at 1,500 rpm and resuspended in Tyrode's solution supplement with elastase (2.4 u/mL), collagenase (250 u/mL), and trypsin inhibitor (10,000 u/mL). The digested vessels were centrifuged, and the pellet of VSMCs was resuspended in the Dulbecco's Modified Eagle's Medium (DMEM, Thermo Scientific, Waltham, MA) containing 20% fetal bovine serum and 1% penicillin/streptomycin. The cells were seeded into a 6-well plate pre-coated with Cell-Tak Cell and Tissue Adhesive (354242, 3.5 μg/cm^2; Corning Inc. Corning, NY) for stocking cells for later experiments or frozen in liquid nitrogen. Early passages (P_2 - P_4) of primary VSMCs were used in all experiments.

Human brain microvascular pericytes (HBMVPs) were purchased from Angio-proteomie (cAP-0030, Boston, MA). Early passages (P_3-P_4) of HBMVPs were seeded in a cell culture plate pre-coated with Cell-Tak Cell and Tissue Adhesive and incubated in pericyte growth medium (cAP-09, Angio-proteomie) for the following experiments. The purity of pericytes

has been validated by staining with several widely accepted markers in our recent study, and > 95% of these cells express α-SMA [50].

2.3. Validation of CYP4A expression in cerebral VSMCs and HBMVPs

The expression of CYP4A in cerebral VSMCs and HBMVPs was determined using immunocytochemistry as we described previously [50, 54–56, 58]. Briefly, primary cerebral VSMCs and HBMVPs were seeded on 4-well Nunc™ Lab-Tek™ II Chamber Slide (154526, Thermo Scientific) pre-coated with Cell-Tak Cell and Tissue Adhesive. The cells were fixed with 3.7% paraformaldehyde (PFA) and subsequently blocked with 1% bovine serum albumin (BSA) after permeabilization with 0.1% Triton-100 (Sigma-Aldrich, St. Louis, MO). The cells were then co-incubated with anti-α-SMA (1: 300; A2547, Sigma-Aldrich) and anti-CYP4A (1: 200; 299230, Daiichi Pure Chemicals, Tokyo, Japan) primary antibodies in a blocking solution at 4 °C overnight, followed by incubation with Alexa Fluor 555 (1: 1,000; A-31570, Thermo Fisher Scientific, Waltham, MA) and Alexa Fluor 488 (1: 1,000; A-11055, Thermo Fisher Scientific)-labeled secondary antibodies at room temperature. The slides were then coverslipped with antifade mounting medium containing 4′,6-diamidino-2-phenylindole (DAPI; H-1200, Vector Laboratories, Burlingame, CA). Images were captured using a Nikon $C2^+$ laser scanning confocal head mounted on an Eclipse Ti2 inverted microscope (Nikon, Melville, NY) with a 20 X objective and 2 X digital zoom (total magnification of 880 X). Experiments using primary VSMCs and HBMVPs were repeated 3–4 times in triplicates.

2.4. Cell Contraction Assay

Cell contractile capability was compared in primary VSMCs and HBMVPs treated with WIT003 or HET0016 following the protocol provided by a collagen gel-based cell contraction assay kit (CBA-201, Cell Biolabs, San Diego, CA). Briefly, VSMCs or HBMVPs were harvested and resuspended in DMEM or pericyte growth medium at a density of 2×10^6 cells/mL. The cells were then mixed with collagen gel working solution on the ice at a ratio of one in four in volume. The cell-gel mixture solution (0.5 mL, containing 2×10^5 cells) was placed in each well of a 24-well plate and incubated for 1 hour at 37 °C for collagen polymerization. The cells were supplied with an appropriate medium (1 mL) and incubated for 24 hours to develop the contractile force at 37 °C in a 5% CO_2 humidified atmosphere. The cells were co-incubated with β-Nicotinamide adenine dinucleotide 2′-phosphate reduced tetrasodium salt hydrate (NADPH; 1 mM; N7505, Sigma-Aldrich) and HET0016 (10 μM) in the presence or absence of WIT003 (10 μM) or 0.2% ethanol in culture medium as a control since the 10 mM stock solutions of both drugs were diluted in ethanol [51, 52]. After incubation, the stressed matrix was detached from the wall of the plate using a sterile needle to initiate the cell contraction. Changes in the collagen gel area were measured using the equation: contraction (%) = $[(Area_{well} - Area_{gel}) / Area_{well}] \times 100\%$ and quantified with Image J software as we previously described [54–57].

HET0016 and WIT003 were synthesized and provided by Dr. John R. Falck (Departments of Biochemistry and Pharmacology, University of Texas Southwestern Medical Center) [53].

2.5. Isolation of cerebral arteries and arterioles

Cerebral arteries and arterioles were freshly isolated from 3-month male rats following the protocol we described previously [55–57]. Briefly, the rats were euthanized with 4% isoflurane. The MCAs and PAs were dissected in an ice-cold calcium-free physiological salt solution (PSS_{0Ca}), containing 1 % BSA, 119 NaCl, 1.17 $MgSO_4$, 4.7 KCl, 18 $NaHCO_3$, 5 HEPES, 1.18 NaH_2PO_4, 10 glucose, 0.03 EDTA (in mM, pH7.4). The PAs in the Virchow-Robin space [59–62] were identified within the MCA territory. A segment of the PA without branches was dissected for the myogenic response. Some vessels were carefully dissected to keep a small piece of the MCA, penetrating arterioles and as many branches as possible on the PAs (down to the capillary levels) for immunostaining to identify CYP4A expression patterns in mural cells on the vessel wall in the MCA territory. A phase-contrast image of the vascular structure of isolated vessels was first obtained using the Lionheart automated live-cell imager (BioTek Instruments, Inc., Winooski, VT) at a magnification of 20 X prior to using the laser scanning confocal microscope for high-resolution images.

2.6. Identification of CYP4A expression in the cerebral mural cells on the vessel wall in the MCA territory

The freshly isolated vessels were fixed with 3.7% PFA and incubated with mixed primary antibodies of anti-α-SMA (1: 300, A2547, Sigma-Aldrich) and anti-CYP4A (1: 200; 299230, Daiichi Pure Chemicals) in a blocking-permeabilizing-staining solution, containing 10% BSA, 2% Triton X-100, and 0.02% sodium azide, at 4 °C for 24 hours in a free-floating manner as we previously described [56]. After incubation with a mixture of Alexa Fluor 555 (1: 1,000, A-31570, Thermo Scientific) and Alexa Fluor 488 (1: 1,000; A-11055, Thermo Fisher Scientific)-labeled secondary antibodies for 2 hours at room temperature and washed gently with phosphate-buffered saline (PBS), the vessels were transferred with a glass Pasteur pipette and placed on a glass Superfrost Plus Microscope Slide (12–550-15, Thermo Scientific), which allows the vessels electrostatically adhere to the glass without additional coating process. The glass pipettes were pre-rinsed with 1% BSA in PBS to prevent sticking. The vessels were repositioned to display all branches without overlap using a glass capillary (6 in, 1.2 mm OD; 1B120–6, World Precision Instruments, Sarasota, FL) thinned with a micropipette puller (Narishige, Tokyo, Japan) and pre-rinsed with 1% BSA. After applied a DAPI antifade mounting medium with hardening formulation (H-1500–10, Vector Laboratories), the slides were coverslipped, and images were obtained by a Nikon $C2^+$ confocal head mounted on an Eclipse Ti2 inverted microscope using a 60 X oil immersion objective (Nikon).

2.7. Effects of 20-HETE on Myogenic Response of the PA

Freshly isolated PAs from SD rats were cannulated with glass micropipettes (6 in, 1.2 mm OD; 1B120–6, World Precision Instruments) bathed with 37 °C PSS (PSS_{0Ca} plus 1.6 mM $CaCl_2$ and without EDTA) with 0.2% ethanol (solute for HETE0016 and WIT003) and equilibrated with 21% O_2, 5% CO_2, 74% N_2 in a pressure myography chamber (Living System Instrumentation, Burlington, VT). HET0016 and WIT003 were prepared at stock concentrations of 1 mM and 10 mM in ethanol, respectively [51, 52]. The PAs were pressurized to 10 mmHg for a 30 – 60 min equilibration period to develop a spontaneous

tone [63–65]. Inner diameters (IDs) of the PA in response to an increase in transmural pressure from 10 to 30 mmHg with or without HET0016 (1 μM) were recorded using a digital camera (MU 1000, AmScope) and an IMT-2 inverted microscope (Olympus, Center Valley, PA) with a 20 X objective connected with the myography chamber. The IDs of the PA in response to HET0016 (1 μM) with or without WIT003 (10 μM) at 30 mmHg were recorded at 5, 10, 15, and 20 min after drug administration. At the end of the experiment, transmural pressure was reset to 10 mmHg. The PAs were washed 6 – 8 times with PSS_{0Ca}, and the IDs of the PA were determined at 10 to 30 mmHg as described above. The myogenic response of PA, isolated from SS, SS.BN5 and SS.*Cyp4a1* rats, was also compared when pressure was increased from 10 to 60 mmHg.

2.8. Effects of 20-HETE on Autoregulation of CBF

The impact of 20-HETE on autoregulation of surface and deep cortical CBF in SD rats was determined with the treatment of HET0016 following the procedure described previously [16, 55, 56, 66]. Briefly, the rats were anesthetized with ketamine (30 mg/kg) and inactin (50 mg/kg). After the trachea was cannulated, the animals were connected to a ventilator (SAR-830, CWE Inc. Ardmore, PA). CO_2 level (30–35 mmHg) was monitored and controlled by a CO_2 analyzer (CAPSTAR-100, CWE Inc.). The femoral artery and vein were implanted with cannulas for mean arterial pressure (MAP) determination and drug delivery. The rat head was placed in a stereotaxic apparatus (model 900, David Kopf, Tujunga, CA), and a thin translucent cranial window was formed using a low-speed air drill. One fiber-optic probe (91–00124, Perimed Inc., Las Vegas, NV) coupled with a laser-Doppler flowmeter (LDF, PF5010, Perimed Inc.) probe was inserted into the brain up to 1.5 – 2 mm for recording the deep cortical CBF [56, 67]. After sealed the open cranial window with bone-wax, another fiber-optic probe was placed above the area without visible vessels within the cranial windows to determine surface cortical CBF. Physiological baseline MAP and CBF on the surface and deep cortex were recorded, and vehicle or HET0016 (2 mg/kg) was slowly infused via the femoral vein. MAP and CBF were recorded at 15 min intervals for 45 mins. MAP was then adjusted to 100 mmHg as experimental baselines. CBF on the surface and deep cortex were recorded as pressures were increased from 100 to 180 mmHg in steps of 20 mmHg by phenylephrine infusion (0.5 – 5 μg/min) via the femoral vein. A steady-state CBF was achieved and recorded by maintaining MAP for 5 mins at each stage. The MAP returned to 100 mmHg by withdrawing phenylephrine to obtain a new baseline LDF. CBF was recorded at each stage of MAP reduced from 100 to 40 mmHg by graded hemorrhage in steps of 20 mmHg.

HET0016 was freshly prepared for every *in vivo* experiment following a protocol that was previously reported [68]. Briefly, a working solution composes of an aliquot of 50 μL of HET0016, dissolved in dimethyl sulfoxide (DMSO) at a concentration of 14 mg/mL, mixed with 950 μL of 30% 2-hydroxy propyl-β-cyclodextrin (HPβCD, prepared in sterile water). Final concentrations of DMSO (5%) and HPβCD (28.5%) in working solution were within maximum tolerated doses for nonclinical vehicles in rat *in vivo* studies that were previously validated in nonclinical safety assessment studies by four research organizations [69].

2.9. Effects of 20-HETE on CBF

To visualize microvessels under two-photon laser-scanning microscopy (TPLSM), the SD rats were anesthetized with 1.5 – 2% isoflurane and a 30: 70 mixture of O_2 and N_2. A thinned cranial window [70, 71] was prepared for TPLSM as previously described [72]. A thin circular area of the skull (~ 2 mm in diameter and ~ 0.5 mm in thickness) 1 mm lateral to the bregma was made using a high-speed microdrill with constant saline irrigation.

Rats were placed in a stereotaxic device on the stage of the TPLSM. Low molecular weight fluorescein isothiocyanate (FITC)-dextran (0.2 mg/kg, IV; Sigma-Aldrich) was injected before imaging. CBF was estimated by measuring red blood cell (RBC) velocities, which were recorded in cortical microvessels (15 – 25 μm ID) 100–150 μm below the surface of the brain before and after HET0016 infusion. The relative CBF was then analyzed using ImageJ analysis software by calculating the slope of the dark lines. Five to ten RBCs traversing at a point in time of the line scans in 8 −11 vessels in three rats were averaged.

2.10. Statistics

All statistical analyses were performed with GraphPad Prism 8 (GraphPad Software, Inc., La Jolla, CA). Results are presented as mean values ± SEM. Significances between groups/strains in corresponding values in cell contraction assay, myogenic response, and CBF autoregulation were compared with a two-way ANOVA for repeated measures followed by a Holm-Sidak *post hoc* test as described previously [66, 73, 74]. The significances in corresponding values of changes in the IDs of the PA, CBF, and CBF autoregulation before and after drug treatments were compared using a paired *t*-test. $P < 0.05$ was considered statistically significant.

3. Results

3.1. CYP4A is expressed in rat cerebral VSMCs and pericytes that express α-SMA

We first confirmed that CYP4A and α-SMA are coexpressed in primary cerebral VSMCs isolated from male SD rats (Figure 1A). We also found that CYP4A is expressed in a human cerebral pericyte cell line that is α-SMA positive, consistent with our previous report (Figure 1B). No nonspecific fluorescence was detected when applied with Alexa Fluor 555 and 488-conjugated 2nd antibodies only in both VSMCs and pericytes (Data not shown).

3.2. CYP4A expression pattern in the cerebral mural cells on the vessel wall in the MCA territory

A represented phase-contrast image of the vascular structure and organization of isolated vessels in the MCA territory is shown in Figure 2A. These arterioles include penetrating arterioles (when branching off from the MCA) and PAs (when entering the brain parenchyma) [57, 60, 62, 75]. The fluid-filled Virchow–Robin space surrounding cerebral microvessels [76, 77] allowed these vessels to be microdissected down to capillary levels without damaging mural cells on the vessel wall.

We found that CYP4A and α-SMA were coexpressed in VSMCs of the arterioles downstream of the MCA of male SD rats (Figure 2B). CYP4A was also found expressed in

all three subtypes of cerebral pericytes, previously defined as ensheathing, mesh, and thin-strand pericytes in mice [39–41]. The expression of α-SMA was found in the arteries, arterioles, and capillaries (Figure 2C). Strong coexpression of α-SMA and CYP4A was detected in most ensheathing and mesh pericytes on the wall of arterioles (ID ~ 20 μm) and capillaries (ID < 10 μm) (Figure 2D–a). However, not all mesh pericytes at arteriolar and capillary junctions expressed α-SMA (Figure 2D–b, Video 1, 2). Two types of thin-strand pericytes were found on the wall of arterioles and capillaries: long thin processes longitudinally coursed along the vessels (Figure 2E–a) or wrapped encompass the vessels (sphincters) (Figure 2E–b); most of these pericytes both expressed α-SMA and CYP4A at the arterioles, but heterogeneity was found at the capillary levels (Figure 2E–b, Video 3). Three to four vessel clusters from four rats were studied. No nonspecific fluorescence was detected when the vessels were incubated with Alexa Fluor 555 and 488-labeled 2nd antibodies only; however, weak autofluorescence was detected but only at the artery and arteriole levels (Data not shown).

3.3. Impact of 20-HETE on cerebral VSMC and pericyte contractile capability

The effects of HET0016 and WIT003 on cerebral VSMC contraction are presented in Figure 3A. Gel size was reduced to a lesser extent in HET0016-treated compared with NADPH-treated (control) cells (17.6 ± 0.4 % vs. 28.3 ± 0.5 %), indicating loss of contractile capability after blockade of 20-HETE. In contrast, WIT003 restored VSMC constriction in HET0016 treated cells with a reduced gel size by 29.7 ± 1.0 %. Similarly, as presented in Figure 3B, the HBMVPs treated with HET0016 without or with WIT003 exhibited a weaker or stronger contractile capability, respectively, compared to control cells incubated with NADPH only, as the gel sizes decreased by 21.5 ± 1.0 % and increased by 31.6 ± 0.6 %, respectively, compared to 28.6 ± 0.9 %.

3.4. Impact of 20-HETE on the myogenic response of the PA

Myogenic response of the PA in SD rats in response to HET0016 and WIT003 were compared. As presented in Figure 4A, the PA constricted by 10.2 ± 0.9 % and 17.8 ± 1.5 % when perfusion pressure was increased from 10 to 20 and 30 mmHg, respectively, indicating an intact myogenic response. Administration of HET0016, a 20-HETE synthesis inhibitor, abolished the pressure-induced vasoconstriction of the PA and the vessels dilated by 13.7 ± 4.9 % and 24.1 ± 1.2 %, respectively when perfusion pressure was elevated over the same range. In another group, the PA exhibited maximal dilation by 34.0 ± 3.3 % at 20 min time point after treatment with HET0016 at 30 mmHg. The vasodilation evoked by HET0016 was rescued by WIT003, a 20-HETE analog, and the PA constricted maximally by 23.3 ± 3.6 %, 10 min after at the same perfusion pressure (Figure 4B).

We also compared the myogenic response of PA of SS, SS.BN5 and SS. *Cyp4a1* rats (Figure 4C). The PA constricted by 18.78 ± 4.13 %, 17.42 ± 4.04 %, and 8.36 ± 5.24 % in SS.BN5, SS.*Cyp4a1,* and SS rats, respectively, when perfusion pressure increased from 10 to 30 mmHg. The PA dilated by 2.94 ± 2.27 %, 2.01 ± 3.34 %, and 30.13 ± 8.35 % in SS.BN5, SS.*Cyp4a1,* and SS rats, respectively, when perfusion pressure increased from to 60 mmHg. Forced dilatation was only found in the PAs of SS rats at pressures > 30 mmHg.

3.5. Impact of 20-HETE on autoregulation of CBF in the Superficial and deep cortex

Surface and deep cortical CBF under physiological baseline MAP and CBF autoregulation in response to HET0016 were compared. MAP was not changed in rats for up to 45 min after administration of vehicle or HET0016 (data not shown).

Surface cortical CBF did not change in the vehicle-treated group, but it significantly increased by 21.5 ± 5.2 % at 30 min and 25.3 ± 5.5 % at 45 min in rats after HET0016 administration (Figure 5A). Deep cortical CBF also increased significantly by 14.6 ± 3.5 % and 16.9 ± 2.6 %, respectively, in HET0016-treated rats at 30 and 45 min after drug administration (Figure 5B). Similarly, the relative CBF, estimated by RBC velocities of cortical microvessels using TPLSM, was increased by 50.86 ± 20.17 % after 30 min HET0016 treatment in SD rats (Figure 5C).

As depicted in Figure 5D and 5E, surface and deep cortical CBF autoregulation in 3-month-old male SD rats infused with vehicle were similar as we recently reported [55, 56] with CBF increasing by 12.9 ± 1.7 % and 13.3 ± 1.9 %, respectively, when MAP was elevated from 100 to 140 mmHg. Surface and deep cortical CBF in control rats increased by 36.2 ± 5.0 % and 34.9 ± 3.9 %, respectively, when pressure was increased beyond the autoregulatory range at 180 mmHg; and decreased by 13.6 ± 2.8 % and 13.8 ± 2.6 %, respectively, at 40 mmHg. In contrast, surface and deep cortical CBF in HET0016-treated rats was increased by 34.6 ± 3.2 % and 28.5 ± 2.3 %, respectively, at 140 mmHg; increased by 79.8 ± 5.4 % and 72.1 ± 8.2 %, respectively, at 180 mmHg; and decreased by 33.4 ± 4.6 % and 26.8 ± 5.7 %, respectively, at 40 mmHg.

Discussion

Emerging evidence over 30 years in human and animal studies demonstrates that 20-HETE exhibits diverse effects in renal and vascular function and plays a pivotal role in hypertension and cardiovascular disease [1, 4–6, 78, 79]. 20-HETE is a product of arachidonic acid catalyzed by the enzymes of CYP4As and CYP4Fs in VSMCs, ECs, pericytes, astrocytes, neurons, and podocytes [31–36]. In the kidney, it inhibits sodium reabsorption and activity of Na^+/K^+-ATPase in the proximal tubule (PT) and thick ascending limb of Henle (TALH) [3, 5, 80], and activates transient receptor potential canonical 6 in podocytes contributing to the modulation of glomerular function [36]. In the vasculature, 20-HETE production is inhibited by superoxide, nitric oxide, and carbon monoxide via activation of potassium channels [81]. On the other hand, 20-HETE evokes vasoconstriction and enhances vascular tone by inhibiting potassium channels [13, 82], activating transient receptor potential [83, 84] and calcium channels [85], as well as protein kinase C, Rho- and tyrosine-kinases [86, 87] to enhance intracellular calcium levels.

A substantial body of evidence has suggested that impaired myogenic response and autoregulation in the cerebral circulation is a common pathogenetic neurovascular pathway that plays an essential role in stroke and dementia and in individuals with aging, hypertension, diabetes, and after traumatic brain or spinal cord injuries [56, 88–95]. CBF autoregulation protects the brain from BBB leakage and swelling in response to elevations in blood pressure [60, 96, 97]. One of the predominant regulators of CBF autoregulation is the

myogenic response, which evokes vasoconstriction in response to elevations in intraluminal pressure. The myogenic response is an intrinsic property of the VSMCs [98] and pericytes [49]; however, not all cerebrovascular pericytes display constrictive capability [46, 99]. Recent studies from the Shih group canonically defined microvascular pericytes in the mouse cortex based on cell morphology, vascular structure and hierarchy, and the α-SMA content [40, 41]. They demonstrated that, unlike VSMCs that have a ring shape with circumferential processes around arteries or arterioles, pericytes have a protruding ovoid cell body. In the mouse cortex, they found an α-SMA terminus at the 1st to 4th order branches ramifying from the penetrating arterioles. Ensheathing pericytes are localized upstream of the α-SMA terminus, but the mesh and thin-strand pericytes are typically localized downstream of the α-SMA terminus. This observation was recently confirmed [43] that α-SMA-enriched sphincters are localized up to the 4th order capillaries in mice cerebral cortex. These sphincter cells exhibited pericyte morphology, which expressed α-SMA. Pericytes that positively express α-SMA regulated CBF, protecting downstream capillaries from elevated perfusion pressure and limiting vasodilation. These cells particularly play a vital role in the regulation of CBF and blood distribution when they localized at the proximal bifurcations of PAs of capillaries [43], which was consistent with a recent report by Gonzales et al., in mice retinal arterioles and capillaries [42, 47] and by our group in cerebral microvessels in rats [31].

Interestingly, results in the present studies in rats are somewhat different from what has been previously reported in mice. We found that there was no clearly defined pattern of the α-SMA terminus in mural cells on the vessel wall in the MCA territory in freshly dissected vessels of 3-month old male SD rats. The expression of α-SMA could be found in mural cells in the arterioles and capillaries. In mice [41], ensheathing pericytes appeared in the PAs and precapillary arterioles upstream of the α-SMA terminus, while mesh pericytes were α-SMA negative that appeared in capillaries only. Notably, ensheathing and mesh pericytes could not be distinguished in rats following such criteria since the “ensheathing” structure at 440 X magnification (Figure 2C) became “mesh” when imaging at 2,640 X (Figure 2D–a). Most of these cells expressed α-SMA, spreading from large arterioles to capillaries since there is no clearly defined α-SMA terminus. However, mesh pericytes that did not express α-SMA were also found, mostly at the arteriolar and capillary junctions (Figure 2D–b, Video 1, 2). Another interesting finding in rats is that the thin-strand pericytes, defined in mice studies, were also found expressing α-SMA and localized on the wall of arterioles and capillaries. These pericytes exhibited long thin processes longitudinally coursed along the vessels as in mice. We also found these pericytes wrapped around and encompassed the vessels, similar to the sphincters but predominantly localized on capillaries (Figure 2E), consistent with our previous report [31]. However, heterogeneity was found at the capillary levels in terms of the coexpression of α-SMA and CYP4A, although most of these pericytes were detected on arterioles (Figure 2E–b, Video 3). We cannot explain why there are two types of thin-strand pericytes found in SD rats in the present studies and in our previous report [31], which are differ from studies in mice [41]. Obviously, our studies utilized rats compared to mice that Shin and other groups used. Of note, our results obtained from isolated PAs within the MCA territory and brain slices [31] in comparison with optically cleared mouse cortex in a PA-capillary bed derived from an un-defined artery [41] or mouse

retinal arteriole-capillary networks [42]. Grubb et al. used TPLSM and identified "precapillary sphincters" in mouse cerebral cortex. However, the TPLSM can reach up to 1 mm depth from the surface of the brain [100] and cannot obtain data from PAs and capillarys at the same time in the same vascular territory.

We found that CYP4A was expressed in VSMCs and α-SMA positive pericytes at arteriolar levels on the vessel wall in the MCA territory in isolated vessels from rats. The present studies revealed that 20-HETE has a direct impact on cerebral VSMC and pericyte cell contractile capability. Inhibition of 20-HETE production reduced cell constriction in both cell types. These effects were rescued by WIT003. We also found that inhibition of 20-HETE production with HET0016 abolished pressure-induced constriction in the PA of SD rats. The vasodilation effects of HET0016 were rescued by WIT003 in these vessels. These results are in line with our early studies using SS rats, a salt-sensitive hypertensive rat model with a genetic deficiency in the production of 20-HETE and the expression of CYP4A [15]. SS rats exhibited reduced myogenic response of the MCA and poor CBF autoregulation on the surface of the brain cortex [16]. The impairments of cerebral vascular hemodynamics were rescued by transferring BN chromosome 5 containing the *Cyp4a* genes and knocking in wildtype *Cyp4a1* onto the SS transgenic background. CYP4A expression and 20-HETE production were globally enhanced, including cerebral vasculature in this model [16]. In the present study, we found that the myogenic response of PA of SS was impaired but was restored in SS.BN5 and SS.*Cyp4a1* rats, similarly as previous results obtained from MCA. The current *in vivo* studies demonstrated that inhibition of 20-HETE synthesis diminished CBF autoregulation in both the surface and deep cortex, and the relative CBF was enhanced in HET0016-treated SD rats, further confirming the direct impacts of 20-HETE on cell contractile capability in cerebral VSMCs and pericytes play an important role in the regulation of CBF. We make the above conclusion that 20-HETE, but not 19-HETE, another arachidonic acid product catalyzed by several CYP4A enzymes is based on previous reports that 19-HETE itself has no effect on vessel diameter but rather acts as a 20-HETE antagonist [53, 101]. Additionally, we used a 20-HETE synthesis inhibitor and an agonist downstream CYP4 enzymes in the 20-HETE pathway, as well as genetically modified rat models.

Poor CBF autoregulation has been found to accelerate detrimental cerebrovascular consequences in aging and various disease [56, 88–92, 102–105]. We have reported that this impairment could transmit elevated pressure to penetrating arterioles and contribute to cerebral vascular disease in another aging hypertensive rat model [106]. We also have reported that the pathogenetic mechanism in CBF autoregulation was found in an aging diabetic model [56], rats with genetic defects or genetically modified in genes regulating vascular function [57, 66, 107]. Compared with the VSMCs on the MCA, pericytes on the PA exhibit an increased calcium channel activity, the lack of large-conductance Ca^{2+}-activated potassium (BK) channel, and greater myogenic tone at physiological pressures [56, 75]. PAs protect downstream capillaries from BBB leakage and swelling by enhancing the resistance of microvessels in the deep cortex [108]. Contractile pericytes at capillary junctions in mice retinal vasculature regulate branch-specific blood flow by receiving hyperpolarizing signals propagating through the capillary network induced by potassium [42].

Nevertheless, heterogeneity of cerebrovascular pericytes in morphology, localization, α-SMA content could be due to differences in species and approach. However, it is most likely due to the diverse effects of cerebrovascular pericytes and their plasticity in the brain under different genetic and environmental conditions [109, 110]. Pericytes regulate CBF, redistribute capillary blood flow, maintain the BBB integrity, and play many other roles such as angiogenesis and phagocytosis [45, 99, 111–114]. Pericyte constriction in response to a thromboxane A2 analog displayed a nonsimultaneous “on and off” operation [44]. The heterogeneity of the coexpression of α-SMA and CYP4A in pericytes at arteriolar and capillary levels suggests CYP4A in α-SMA negative pericytes at the neurovascular unit may play a different role, which may involve pericyte-endothelia crosstalk to maintain BBB integrity. Indeed, it is under-explored how to define brain pericytes into subtypes in different species under different physiological and pathological conditions, how pericyte heterogeneity and plasticity play different roles, and how pericytes produce, receive and propagate signals to crosstalk with other brain cell types.

Conclusions

Results from the current study indicated, for the first time, that 20-HETE-promoted CBF autoregulation is associated with enhanced α-SMA positive cerebrovascular pericyte contractility in rats. This observation is associated with the coexpression of CYP4A and α-SMA in cerebral VSMCs and most pericytes. Our findings provide a novel insight into possible mechanisms by which inactivating variants of 20-HETE producing enzymes have been found in hypertension, stroke, and AD patients [10, 18–29].

Supplementary Material

Refer to Web version on PubMed Central for supplementary material.

Acknowledgments

Funding

This study was supported by grants AG050049, AG057842, P20GM104357, and HL138685 from the National Institutes of Health.

REFERENCES

[1]. Fan F, Ge Y, Lv W, Elliott MR, Muroya Y, Hirata T, Booz GW, Roman RJ, Molecular mechanisms and cell signaling of 20-hydroxyeicosatetraenoic acid in vascular pathophysiology, Front Biosci (Landmark Ed) 21 (2016) 1427–63. [PubMed: 27100515]

[2]. Fan F, Muroya Y, Roman RJ, Cytochrome P450 eicosanoids in hypertension and renal disease, Curr Opin Nephrol Hypertens 24(1) (2015) 37–46. [PubMed: 25427230]

[3]. Fan F, Roman RJ, Effect of Cytochrome P450 Metabolites of Arachidonic Acid in Nephrology, J Am Soc Nephrol 28(10) (2017) 2845–2855. [PubMed: 28701518]

[4]. Shekhar S, Varghese K, Li M, Fan L, Booz GW, Roman RJ, Fan F, Conflicting Roles of 20-HETE in Hypertension and Stroke, Int J Mol Sci 20(18) (2019) 4500.

[5]. Zhang C, Booz GW, Yu Q, He X, Wang S, Fan F, Conflicting roles of 20-HETE in hypertension and renal end organ damage, Eur J Pharmacol 833 (2018) 190–200. [PubMed: 29886242]

[6]. Roman RJ, Fan F, 20-HETE: Hypertension and Beyond, Hypertension 72(1) (2018) 12–18. [PubMed: 29760152]

[7]. Yabluchanskiy A, Tarantini S, Balasubramanian P, Kiss T, Csipo T, Fülöp GA, Lipecz A, Ahire C, DelFavero J, Nyul-Toth A, Sonntag WE, Schwartzman ML, Campisi J, Csiszar A, Ungvari Z, Pharmacological or genetic depletion of senescent astrocytes prevents whole brain irradiation-induced impairment of neurovascular coupling responses protecting cognitive function in mice, Geroscience 42(2) (2020) 409–428. [PubMed: 31960269]

[8]. Toth P, Tucsek Z, Sosnowska D, Gautam T, Mitschelen M, Tarantini S, Deak F, Koller A, Sonntag WE, Csiszar A, Ungvari Z, Age-related autoregulatory dysfunction and cerebromicrovascular injury in mice with angiotensin II-induced hypertension, J Cereb Blood Flow Metab 33(11) (2013) 1732–42. [PubMed: 23942363]

[9]. Toth P, Csiszar A, Sosnowska D, Tucsek Z, Cseplo P, Springo Z, Tarantini S, Sonntag WE, Ungvari Z, Koller A, Treatment with the cytochrome P450 omega-hydroxylase inhibitor HET0016 attenuates cerebrovascular inflammation, oxidative stress and improves vasomotor function in spontaneously hypertensive rats, Br J Pharmacol 168(8) (2013) 1878–88. [PubMed: 23194285]

[10]. Fan F, Simino J, Auchus AP, Knopman DS, Boerwinkle E, Fornage M, Mosley TH, Roman RJ, Functional variants in CYP4A11 and CYP4F2 are associated with cognitive impairment and related dementia endophenotypes in the elderly, The 16th International Winter Eicosanoid Conference, Baltimore, 2016, p. CV5.

[11]. Muroya Y, Fan F, Regner KR, Falck JR, Garrett MR, Juncos LA, Roman RJ, Deficiency in the Formation of 20-Hydroxyeicosatetraenoic Acid Enhances Renal Ischemia-Reperfusion Injury, J Am Soc Nephrol 26(10) (2015) 2460–9. [PubMed: 25644108]

[12]. Yanes LL, Lima R, Moulana M, Romero DG, Yuan K, Ryan MJ, Baker R, Zhang H, Fan F, Davis D.d., Roman RJ, Reckelhoff JF, Postmenopausal hypertension: role of 20-HETE, Am J Physiol Regul Integr Comp Physiol 300(6) (2011) R1543–8. [PubMed: 21474427]

[13]. Fan F, Sun CW, Maier KG, Williams JM, Pabbidi MR, Didion SP, Falck JR, Zhuo J, Roman RJ, 20-Hydroxyeicosatetraenoic acid contributes to the inhibition of K+ channel activity and vasoconstrictor response to angiotensin II in rat renal microvessels, PLoS One 8(12) (2013) e82482. [PubMed: 24324797]

[14]. Czakó C, Kovács T, Ungvari Z, Csiszar A, Yabluchanskiy A, Conley S, Csipo T, Lipecz A, Horváth H, Sándor GL, István L, Logan T, Nagy ZZ, Kovács I, Retinal biomarkers for Alzheimer's disease and vascular cognitive impairment and dementia (VCID): implication for early diagnosis and prognosis, Geroscience 42(6) (2020) 1499–1525. [PubMed: 33011937]

[15]. Williams JM, Fan F, Murphy S, Schreck C, Lazar J, Jacob HJ, Roman RJ, Role of 20-HETE in the antihypertensive effect of transfer of chromosome 5 from Brown Norway to Dahl salt-sensitive rats, Am J Physiol Regul Integr Comp Physiol 302(10) (2012) R1209–18. [PubMed: 22442195]

[16]. Fan F, Geurts AM, Murphy SR, Pabbidi MR, Jacob HJ, Roman RJ, Impaired myogenic response and autoregulation of cerebral blood flow is rescued in CYP4A1 transgenic Dahl salt-sensitive rat, Am J Physiol Regul Integr Comp Physiol 308(5) (2015) R379–90. [PubMed: 25540098]

[17]. Dunn KM, Renic M, Flasch AK, Harder DR, Falck J, Roman RJ, Elevated production of 20-HETE in the cerebral vasculature contributes to severity of ischemic stroke and oxidative stress in spontaneously hypertensive rats, Am J Physiol Heart Circ Physiol 295(6) (2008) H2455–65. [PubMed: 18952718]

[18]. Deng S, Zhu G, Liu F, Zhang H, Qin X, Li L, Zhiyi H, CYP4F2 gene V433M polymorphism is associated with ischemic stroke in the male Northern Chinese Han population, Prog Neuropsychopharmacol Biol Psychiatry 34(4) (2010) 664–8. [PubMed: 20227456]

[19]. Ding H, Cui G, Zhang L, Xu Y, Bao X, Tu Y, Wu B, Wang Q, Hui R, Wang W, Dackor RT, Kissling GE, Zeldin DC, Wang DW, Association of common variants of CYP4A11 and CYP4F2 with stroke in the Han Chinese population, Pharmacogenet Genomics 20(3) (2010) 187–94. [PubMed: 20130494]

[20]. Fava C, Bonafini S, Eicosanoids via CYP450 and cardiovascular disease: Hints from genetic and nutrition studies, Prostaglandins Other Lipid Mediat 139 (2018) 41–47. [PubMed: 30296490]

[21]. Fava C, Montagnana M, Almgren P, Rosberg L, Lippi G, Hedblad B, Engstrom G, Berglund G, Minuz P, Melander O, The V433M variant of the CYP4F2 is associated with ischemic stroke in

male Swedes beyond its effect on blood pressure, Hypertension 52(2) (2008) 373–80. [PubMed: 18574070]

[22]. Fava C, Ricci M, Melander O, Minuz P, Hypertension, cardiovascular risk and polymorphisms in genes controlling the cytochrome P450 pathway of arachidonic acid: A sex-specific relation?, Prostaglandins Other Lipid Mediat 98(3–4) (2012) 75–85. [PubMed: 22173545]

[23]. Fu Z, Nakayama T, Sato N, Izumi Y, Kasamaki Y, Shindo A, Ohta M, Soma M, Aoi N, Sato M, Matsumoto K, Ozawa Y, Ma Y, A haplotype of the CYP4F2 gene is associated with cerebral infarction in Japanese men, Am J Hypertens 21(11) (2008) 1216–23. [PubMed: 18787519]

[24]. Kim WY, Lee SJ, Min J, Oh KS, Kim DH, Kim HS, Shin JG, Identification of novel CYP4F2 genetic variants exhibiting decreased catalytic activity in the conversion of arachidonic acid to 20-hydroxyeicosatetraenoic acid (20-HETE), Prostaglandins Leukot Essent Fatty Acids 131 (2018) 6–13. [PubMed: 29628049]

[25]. Liao D, Yi X, Zhang B, Zhou Q, Lin J, Interaction Between CYP4F2 rs2108622 and CPY4A11 rs9333025 Variants Is Significantly Correlated with Susceptibility to Ischemic Stroke and 20-Hydroxyeicosatetraenoic Acid Level, Genet Test Mol Biomarkers 20(5) (2016) 223–8. [PubMed: 26959478]

[26]. Munshi A, Sharma V, Kaul S, Al-Hazzani A, Alshatwi AA, Shafi G, Koppula R, Mallemoggala SB, Jyothy A, Association of 1347 G/A cytochrome P450 4F2 (CYP4F2) gene variant with hypertension and stroke, Mol Biol Rep 39(2) (2012) 1677–82. [PubMed: 21625857]

[27]. Stec DE, Roman RJ, Flasch A, Rieder MJ, Functional polymorphism in human CYP4F2 decreases 20-HETE production, Physiol Genomics 30(1) (2007) 74–81. [PubMed: 17341693]

[28]. Ward NC, Tsai IJ, Barden A, van Bockxmeer FM, Puddey IB, Hodgson JM, Croft KD, A single nucleotide polymorphism in the CYP4F2 but not CYP4A11 gene is associated with increased 20-HETE excretion and blood pressure, Hypertension 51(5) (2008) 1393–8. [PubMed: 18391101]

[29]. Zhang B, Yi X, Wang C, Liao D, Lin J, Chi L, Cytochrome 4A11 Genetic Polymorphisms Increase Susceptibility to Ischemic Stroke and Associate with Atherothrombotic Events After Stroke in Chinese, Genet Test Mol Biomarkers 19(5) (2015) 235–41. [PubMed: 25734770]

[30]. Gainer JV, Bellamine A, Dawson EP, Womble KE, Grant SW, Wang Y, Cupples LA, Guo CY, Demissie S, O'Donnell CJ, Brown NJ, Waterman MR, Capdevila JH, Functional variant of CYP4A11 20-hydroxyeicosatetraenoic acid synthase is associated with essential hypertension, Circulation 111(1) (2005) 63–9. [PubMed: 15611369]

[31]. Gonzalez-Fernandez E, Staursky D, Lucas K, Nguyen BV, Li M, Liu Y, Washington C, Coolen LM, Fan F, Roman RJ, 20-HETE Enzymes and Receptors in the Neurovascular Unit: Implications in Cerebrovascular Disease, Front Neurol 11 (2020) 983. [PubMed: 33013649]

[32]. Orozco LD, Liu H, Perkins E, Johnson DA, Chen BB, Fan F, Baker RC, Roman RJ, 20-Hydroxyeicosatetraenoic acid inhibition attenuates balloon injury-induced neointima formation and vascular remodeling in rat carotid arteries, J Pharmacol Exp Ther 346(1) (2013) 67–74. [PubMed: 23658377]

[33]. Guo AM, Janic B, Sheng J, Falck JR, Roman RJ, Edwards PA, Arbab AS, Scicli AG, The cytochrome P450 4A/F-20-hydroxyeicosatetraenoic acid system: a regulator of endothelial precursor cells derived from human umbilical cord blood, J Pharmacol Exp Ther 338(2) (2011) 421–9. [PubMed: 21527533]

[34]. Guo AM, Sheng J, Scicli GM, Arbab AS, Lehman NL, Edwards PA, Falck JR, Roman RJ, Scicli AG, Expression of CYP4A1 in U251 human glioma cell induces hyperproliferative phenotype in vitro and rapidly growing tumors in vivo, J Pharmacol Exp Ther 327(1) (2008) 10–9. [PubMed: 18591218]

[35]. Hoopes SL, Garcia V, Edin ML, Schwartzman ML, Zeldin DC, Vascular actions of 20-HETE, Prostaglandins Other Lipid Mediat 120 (2015) 9–16. [PubMed: 25813407]

[36]. Roshanravan H, Kim EY, Dryer SE, 20-Hydroxyeicosatetraenoic Acid (20-HETE) Modulates Canonical Transient Receptor Potential-6 (TRPC6) Channels in Podocytes, Front Physiol 7 (2016) 351. [PubMed: 27630573]

[37]. Toth P, Csiszar A, Tucsek Z, Sosnowska D, Gautam T, Koller A, Schwartzman ML, Sonntag WE, Ungvari Z, Role of 20-HETE, TRPC channels, and BKCa in dysregulation of pressure-induced

Ca2+ signaling and myogenic constriction of cerebral arteries in aged hypertensive mice, Am J Physiol Heart Circ Physiol 305(12) (2013) H1698–708. [PubMed: 24097425]

[38]. Wang S, Jiao F, Guo Y, Booz G, Roman R, Fan F, Role of Vascular Smooth Muscle Cells in Diabetes-related Vascular Cognitive Impairment, Stroke 50(Suppl_1) (2019) ATP556–ATP556.

[39]. Brown LS, Foster CG, Courtney JM, King NE, Howells DW, Sutherland BA, Pericytes and Neurovascular Function in the Healthy and Diseased Brain, Front Cell Neurosci 13 (2019) 282. [PubMed: 31316352]

[40]. Hartmann DA, Underly RG, Grant RI, Watson AN, Lindner V, Shih AY, Pericyte structure and distribution in the cerebral cortex revealed by high-resolution imaging of transgenic mice, Neurophotonics 2(4) (2015) 041402. [PubMed: 26158016]

[41]. Grant RI, Hartmann DA, Underly RG, Berthiaume AA, Bhat NR, Shih AY, Organizational hierarchy and structural diversity of microvascular pericytes in adult mouse cortex, J Cereb Blood Flow Metab 39(3) (2019) 411–425. [PubMed: 28933255]

[42]. Gonzales AL, Klug NR, Moshkforoush A, Lee JC, Lee FK, Shui B, Tsoukias NM, Kotlikoff MI, Hill-Eubanks D, Nelson MT, Contractile pericytes determine the direction of blood flow at capillary junctions, Proc Natl Acad Sci U S A 117(43) (2020) 27022–27033. [PubMed: 33051294]

[43]. Grubb S, Cai C, Hald BO, Khennouf L, Murmu RP, Jensen AGK, Fordsmann J, Zambach S, Lauritzen M, Precapillary sphincters maintain perfusion in the cerebral cortex, Nat Commun 11(1) (2020) 395. [PubMed: 31959752]

[44]. Fernandez-Klett F, Offenhauser N, Dirnagl U, Priller J, Lindauer U, Pericytes in capillaries are contractile in vivo, but arterioles mediate functional hyperemia in the mouse brain, Proc Natl Acad Sci U S A 107(51) (2010) 22290–5. [PubMed: 21135230]

[45]. Bandopadhyay R, Orte C, Lawrenson JG, Reid AR, De Silva S, Allt G, Contractile proteins in pericytes at the blood-brain and blood-retinal barriers, J Neurocytol 30(1) (2001) 35–44. [PubMed: 11577244]

[46]. Hall CN, Reynell C, Gesslein B, Hamilton NB, Mishra A, Sutherland BA, O'Farrell FM, Buchan AM, Lauritzen M, Attwell D, Capillary pericytes regulate cerebral blood flow in health and disease, Nature 508(7494) (2014) 55–60. [PubMed: 24670647]

[47]. Nehls V, Drenckhahn D, Heterogeneity of microvascular pericytes for smooth muscle type alpha-actin, J Cell Biol 113(1) (1991) 147–54. [PubMed: 2007619]

[48]. Peppiatt CM, Howarth C, Mobbs P, Attwell D, Bidirectional control of CNS capillary diameter by pericytes, Nature 443(7112) (2006) 700–4. [PubMed: 17036005]

[49]. Liu Y, Wang S, Guo Y, Zhang H, Roman RJ, Fan F, Impaired Pericyte Constriction and Cerebral Blood Flow Autoregulationin Diabetes, Stroke 51(Suppl_1) (2020) AWP498–AWP498.

[50]. Liu Y, Zhang H, Wang S, Guo Y, Fang X, Zheng B, Gao W, Yu H, Chen Z, Roman RJ, Fan F, Reduced pericyte and tight junction coverage in old diabetic rats are associated with hyperglycemia-induced cerebrovascular pericyte dysfunction, Am J Physiol Heart Circ Physiol 320(2) (2021) H549–h562. [PubMed: 33306445]

[51]. Yu M, Cambj-Sapunar L, Kehl F, Maier KG, Takeuchi K, Miyata N, Ishimoto T, Reddy LM, Falck JR, Gebremedhin D, Harder DR, Roman RJ, Effects of a 20-HETE antagonist and agonists on cerebral vascular tone, Eur J Pharmacol 486(3) (2004) 297–306. [PubMed: 14985052]

[52]. Miyata N, Taniguchi K, Seki T, Ishimoto T, Sato-Watanabe M, Yasuda Y, Doi M, Kametani S, Tomishima Y, Ueki T, Sato M, Kameo K, HET0016, a potent and selective inhibitor of 20-HETE synthesizing enzyme, Br J Pharmacol 133(3) (2001) 325–9. [PubMed: 11375247]

[53]. Alonso-Galicia M, Falck JR, Reddy KM, Roman RJ, 20-HETE agonists and antagonists in the renal circulation, Am J Physiol 277(5) (1999) F790–6. [PubMed: 10564244]

[54]. Guo Y, Wang S, Liu Y, Fan L, Booz GW, Roman RJ, Chen Z, Fan F, Accelerated cerebral vascular injury in diabetes is associated with vascular smooth muscle cell dysfunction, Geroscience 42(2) (2020) 547–561. [PubMed: 32166556]

[55]. Wang S, Zhang H, Liu Y, Li L, Guo Y, Jiao F, Fang X, Jefferson JR, Li M, Gao W, Gonzalez-Fernandez E, Maranon RO, Pabbidi MR, Liu R, Alexander BT, Roman RJ, Fan F, Sex differences in the structure and function of rat middle cerebral arteries, Am J Physiol Heart Circ Physiol 318(5) (2020) H1219–H1232. [PubMed: 32216612]

[56]. Wang S, Lv W, Zhang H, Liu Y, Li L, Jefferson JR, Guo Y, Li M, Gao W, Fang X, Paul IA, Rajkowska G, Shaffery JP, Mosley TH, Hu X, Liu R, Wang Y, Yu H, Roman RJ, Fan F, Aging exacerbates impairments of cerebral blood flow autoregulation and cognition in diabetic rats, Geroscience 42(5) (2020) 1387–1410. [PubMed: 32696219]

[57]. Zhang H, Zhang C, Liu Y, Gao W, Wang S, Fang X, Guo Y, Li M, Liu R, Roman RJ, Sun P, Fan F, Influence of dual-specificity protein phosphatase 5 on mechanical properties of rat cerebral and renal arterioles, Physiol Rep 8(2) (2020) e14345. [PubMed: 31960618]

[58]. Gao W, Liu Y, Fan L, Zheng B, Jefferson JR, Wang S, Zhang H, Fang X, Nguyen BV, Zhu T, Roman RJ, Fan F, Role of γ-adducin in actin cytoskeleton rearrangements in podocyte pathophysiology, Am J Physiol Renal Physiol 320(1) (2021) F97–f113. [PubMed: 33308016]

[59]. Shaver SW, Pang JJ, Wainman DS, Wall KM, Gross PM, Morphology and function of capillary networks in subregions of the rat tuber cinereum, Cell and tissue research 267(3) (1992) 437–48. [PubMed: 1571958]

[60]. Cipolla MJ, The Cerebral Circulation, San Rafael (CA): Morgan & Claypool Life Sciences (2009).

[61]. Cipolla MJ, Bullinger LV, Reactivity of brain parenchymal arterioles after ischemia and reperfusion, Microcirculation 15(6) (2008) 495–501. [PubMed: 19086259]

[62]. Pires PW, Dabertrand F, Earley S, Isolation and Cannulation of Cerebral Parenchymal Arterioles, J Vis Exp (111) (2016).

[63]. Harper SL, Bohlen HG, Rubin MJ, Arterial and microvascular contributions to cerebral cortical autoregulation in rats, Am J Physiol 246(1 Pt 2) (1984) H17–24. [PubMed: 6696087]

[64]. Faraci FM, Heistad DD, Regulation of large cerebral arteries and cerebral microvascular pressure, Circ Res 66(1) (1990) 8–17. [PubMed: 2403863]

[65]. Mayhan WG, Heistad DD, Role of veins and cerebral venous pressure in disruption of the blood-brain barrier, Circ Res 59(2) (1986) 216–20. [PubMed: 3742745]

[66]. Fan F, Geurts AM, Pabbidi MR, Smith SV, Harder DR, Jacob H, Roman RJ, Zinc-finger nuclease knockout of dual-specificity protein phosphatase-5 enhances the myogenic response and autoregulation of cerebral blood flow in FHH.1BN rats, PLoS One 9(11) (2014) e112878. [PubMed: 25397684]

[67]. Korbo L, Pakkenberg B, Ladefoged O, Gundersen HJ, Arlien-Soborg P, Pakkenberg H, An efficient method for estimating the total number of neurons in rat brain cortex, Journal of neuroscience methods 31(2) (1990) 93–100. [PubMed: 2181205]

[68]. Jain M, Gamage NH, Alsulami M, Shankar A, Achyut BR, Angara K, Rashid MH, Iskander A, Borin TF, Wenbo Z, Ara R, Ali MM, Lebedyeva I, Chwang WB, Guo A, Bagher-Ebadian H, Arbab AS, Intravenous Formulation of HET0016 Decreased Human Glioblastoma Growth and Implicated Survival Benefit in Rat Xenograft Models, Sci Rep 7 (2017) 41809. [PubMed: 28139732]

[69]. Gad SC, Cassidy CD, Aubert N, Spainhour B, Robbe H, Nonclinical vehicle use in studies by multiple routes in multiple species, Int J Toxicol 25(6) (2006) 499–521. [PubMed: 17132609]

[70]. Lin HW, Gresia VL, Stradecki HM, Alekseyenko A, Dezfulian C, Neumann JT, Dave KR, Perez-Pinzon MA, Protein kinase C delta modulates endothelial nitric oxide synthase after cardiac arrest, J Cereb Blood Flow Metab 34(4) (2014) 613–20. [PubMed: 24447953]

[71]. Xu HT, Pan F, Yang G, Gan WB, Choice of cranial window type for in vivo imaging affects dendritic spine turnover in the cortex, Nat Neurosci 10(5) (2007) 549–51. [PubMed: 17417634]

[72]. Yang G, Pan F, Parkhurst CN, Grutzendler J, Gan WB, Thinned-skull cranial window technique for long-term imaging of the cortex in live mice, Nat Protoc 5(2) (2010) 201–8. [PubMed: 20134419]

[73]. Fan F, Geurts AM, Pabbidi MR, Ge Y, Zhang C, Wang S, Liu Y, Gao W, Guo Y, Li L, He X, Lv W, Muroya Y, Hirata T, Prokop J, Booz GW, Jacob HJ, Roman RJ, A Mutation in gamma-Adducin Impairs Autoregulation of Renal Blood Flow and Promotes the Development of Kidney Disease, J Am Soc Nephrol 31(4) (2020) 687–700. [PubMed: 32029431]

[74]. Fan F, Pabbidi MR, Ge Y, Li L, Wang S, Mims PN, Roman RJ, Knockdown of Add3 impairs the myogenic response of renal afferent arterioles and middle cerebral arteries, Am J Physiol Renal Physiol 312(6) (2017) F971–F981. [PubMed: 27927653]

[75]. Cipolla MJ, Sweet J, Chan SL, Tavares MJ, Gokina N, Brayden JE, Increased pressure-induced tone in rat parenchymal arterioles vs. middle cerebral arteries: role of ion channels and calcium sensitivity, J Appl Physiol (1985) 117(1) (2014) 53–9. [PubMed: 24790017]

[76]. Esiri MM, Gay D, Immunological and neuropathological significance of the Virchow-Robin space, J Neurol Sci 100(1–2) (1990) 3–8. [PubMed: 2089138]

[77]. Owens T, Bechmann I, Engelhardt B, Perivascular spaces and the two steps to neuroinflammation, J Neuropathol Exp Neurol 67(12) (2008) 1113–21. [PubMed: 19018243]

[78]. Fan F, Roman RJ, GPR75 Identified as the First 20-HETE Receptor: A Chemokine Receptor Adopted by a New Family, Circ Res 120(11) (2017) 1696–1698. [PubMed: 28546348]

[79]. Roman RJ, P-450 metabolites of arachidonic acid in the control of cardiovascular function, Physiol Rev 82(1) (2002) 131–85. [PubMed: 11773611]

[80]. Yu M, Lopez B, Dos Santos EA, Falck JR, Roman RJ, Effects of 20-HETE on Na+ transport and Na+ -K+ -ATPase activity in the thick ascending loop of Henle, Am J Physiol Regul Integr Comp Physiol 292(6) (2007) R2400–5. [PubMed: 17303679]

[81]. Sun CW, Alonso-Galicia M, Taheri MR, Falck JR, Harder DR, Roman RJ, Nitric oxide-20-hydroxyeicosatetraenoic acid interaction in the regulation of K+ channel activity and vascular tone in renal arterioles, Circ Res 83(11) (1998) 1069–79. [PubMed: 9831701]

[82]. Zou AP, Fleming JT, Falck JR, Jacobs ER, Gebremedhin D, Harder DR, Roman RJ, 20-HETE is an endogenous inhibitor of the large-conductance Ca(2+)-activated K+ channel in renal arterioles, Am J Physiol 270(1 Pt 2) (1996) R228–37. [PubMed: 8769806]

[83]. Brayden JE, Earley S, Nelson MT, Reading S, Transient receptor potential (TRP) channels, vascular tone and autoregulation of cerebral blood flow, Clin Exp Pharmacol Physiol 35(9) (2008) 1116–20. [PubMed: 18215190]

[84]. Wen H, Ostman J, Bubb KJ, Panayiotou C, Priestley JV, Baker MD, Ahluwalia A, 20-Hydroxyeicosatetraenoic acid (20-HETE) is a novel activator of transient receptor potential vanilloid 1 (TRPV1) channel, J Biol Chem 287(17) (2012) 13868–76. [PubMed: 22389490]

[85]. Gebremedhin D, Lange AR, Narayanan J, Aebly MR, Jacobs ER, Harder DR, Cat cerebral arterial smooth muscle cells express cytochrome P450 4A2 enzyme and produce the vasoconstrictor 20-HETE which enhances L-type Ca2+ current, J Physiol 507 (Pt 3) (1998) 771–81. [PubMed: 9508838]

[86]. Sun CW, Falck JR, Harder DR, Roman RJ, Role of tyrosine kinase and PKC in the vasoconstrictor response to 20-HETE in renal arterioles, Hypertension 33(1 Pt 2) (1999) 414–8. [PubMed: 9931139]

[87]. Parmentier JH, Muthalif MM, Saeed AE, Malik KU, Phospholipase D activation by norepinephrine is mediated by 12(s)-, 15(s)-, and 20-hydroxyeicosatetraenoic acids generated by stimulation of cytosolic phospholipase a2. tyrosine phosphorylation of phospholipase d2 in response to norepinephrine, J Biol Chem 276(19) (2001) 15704–11. [PubMed: 11278912]

[88]. Shekhar S, Wang S, Mims PN, Gonzalez-Fernandez E, Zhang C, He X, Liu CY, Lv W, Wang Y, Huang J, Fan F, Impaired Cerebral Autoregulation-A Common Neurovascular Pathway in Diabetes may Play a Critical Role in Diabetes-Related Alzheimer's Disease, Curr Res Diabetes Obes J 2(3) (2017) 555587. [PubMed: 28825056]

[89]. Shekhar S, Liu R, Travis OK, Roman RJ, Fan F, Cerebral Autoregulation in Hypertension and Ischemic Stroke: A Mini Review, J Pharm Sci Exp Pharmacol 2017(1) (2017) 21–27. [PubMed: 29333537]

[90]. Wang S, Roman RJ, Fan F, Duration and magnitude of bidirectional fluctuation in blood pressure: the link between cerebrovascular dysfunction and cognitive impairment following spinal cord injury, J Neurobiol Physiol 2(1) (2020) 15–18. [PubMed: 33336208]

[91]. Ungvari Z, Tarantini S, Donato AJ, Galvan V, Csiszar A, Mechanisms of Vascular Aging, Circ Res 123(7) (2018) 849–867. [PubMed: 30355080]

[92]. Sachdeva R, Jia M, Wang S, Yung A, Zheng MMZ, Lee AHX, Monga A, Leong S, Kozlowski P, Fan F, Roman RJ, Phillips AA, Krassioukov AV, Vascular-Cognitive Impairment following High-Thoracic Spinal Cord Injury Is Associated with Structural and Functional Maladaptations in Cerebrovasculature, Journal of neurotrauma 37(18) (2020) 1963–1970. [PubMed: 32394805]

[93]. Ungvari Z, Tarantini S, Hertelendy P, Valcarcel-Ares MN, Fülöp GA, Logan S, Kiss T, Farkas E, Csiszar A, Yabluchanskiy A, Cerebromicrovascular dysfunction predicts cognitive decline and gait abnormalities in a mouse model of whole brain irradiation-induced accelerated brain senescence, Geroscience 39(1) (2017) 33–42. [PubMed: 28299642]

[94]. Tarantini S, Yabluchanskiy A, Csipo T, Fulop G, Kiss T, Balasubramanian P, DelFavero J, Ahire C, Ungvari A, Nyúl-Tóth Á, Farkas E, Benyo Z, Tóth A, Csiszar A, Ungvari Z, Treatment with the poly(ADP-ribose) polymerase inhibitor PJ-34 improves cerebromicrovascular endothelial function, neurovascular coupling responses and cognitive performance in aged mice, supporting the NAD+ depletion hypothesis of neurovascular aging, Geroscience 41(5) (2019) 533–542. [PubMed: 31679124]

[95]. Young AP, Zhu J, Bagher AM, Denovan-Wright EM, Howlett SE, Kelly MEM, Endothelin B receptor dysfunction mediates elevated myogenic tone in cerebral arteries from aged male Fischer 344 rats, Geroscience (2021).

[96]. Wiedenhoeft T, Tarantini S, Nyúl-Tóth Á, Yabluchanskiy A, Csipo T, Balasubramanian P, Lipecz A, Kiss T, Csiszar A, Csiszar A, Ungvari Z, Fusogenic liposomes effectively deliver resveratrol to the cerebral microcirculation and improve endothelium-dependent neurovascular coupling responses in aged mice, Geroscience 41(6) (2019) 711–725. [PubMed: 31654270]

[97]. Kim KJ, Diaz JR, Presa JL, Muller PR, Brands MW, Khan MB, Hess DC, Althammer F, Stern JE, Filosa JA, Decreased parenchymal arteriolar tone uncouples vessel-to-neuronal communication in a mouse model of vascular cognitive impairment, Geroscience (2021).

[98]. Bayliss WM, On the local reactions of the arterial wall to changes of internal pressure, J Physiol 28(3) (1902) 220–31. [PubMed: 16992618]

[99]. Armulik A, Genove G, Betsholtz C, Pericytes: developmental, physiological, and pathological perspectives, problems, and promises, Dev Cell 21(2) (2011) 193–215. [PubMed: 21839917]

[100]. Denk W, Strickler J, Webb W, Two-photon laser scanning fluorescence microscopy, Science 248(4951) (1990) 73–76. [PubMed: 2321027]

[101]. Dakarapu R, Errabelli R, Manthati VL, Michael Adebesin A, Barma DK, Barma D, Garcia V, Zhang F, Laniado Schwartzman M, Falck JR, 19-Hydroxyeicosatetraenoic acid analogs: Antagonism of 20-hydroxyeicosatetraenoic acid-induced vascular sensitization and hypertension, Bioorganic & medicinal chemistry letters 29(19) (2019) 126616. [PubMed: 31439380]

[102]. Csiszar A, Yabluchanskiy A, Ungvari A, Ungvari Z, Tarantini S, Overexpression of catalase targeted to mitochondria improves neurovascular coupling responses in aged mice, Geroscience 41(5) (2019) 609–617. [PubMed: 31643012]

[103]. Sure VN, Sakamuri S, Sperling JA, Evans WR, Merdzo I, Mostany R, Murfee WL, Busija DW, Katakam PVG, A novel high-throughput assay for respiration in isolated brain microvessels reveals impaired mitochondrial function in the aged mice, Geroscience 40(4) (2018) 365–375. [PubMed: 30074132]

[104]. Tarantini S, Yabluchanksiy A, Fülöp GA, Hertelendy P, Valcarcel-Ares MN, Kiss T, Bagwell JM, O'Connor D, Farkas E, Sorond F, Csiszar A, Ungvari Z, Pharmacologically induced impairment of neurovascular coupling responses alters gait coordination in mice, Geroscience 39(5–6) (2017) 601–614. [PubMed: 29243191]

[105]. Soleimanzad H, Montaner M, Ternier G, Lemitre M, Silvestre JS, Kassis N, Giacobini P, Magnan C, Pain F, Gurden H, Obesity in Midlife Hampers Resting and Sensory-Evoked Cerebral Blood Flow in Mice, Obesity (Silver Spring) (2020).

[106]. Fan F, Pabbidi M, Lin RCS, Ge Y, Gomez-Sanchez EP, Rajkowska GK, Moulana M, Gonzalez-fernandez E, Sims J, Elliott MR, Paul IA, Alexander AP, Mosley TH, Harder DR, Roman RJ, Impaired myogenic response of MCA elevates transmission of pressure to penetrating arterioles and contributes to cerebral vascular disease in aging hypertensive FHH rats, The FASEB Journal 30(S1) (2016) 953.7–953.7.

[107]. Fan F, Wang SX, Mims PN, Maeda KJ, Li LY, Geurts AM, Roman RJ, Knockout of matrix metalloproteinase-9 rescues the development of cognitive impairments in hypertensive Dahl salt sensitive rats, FASEB J 31(1_supplement) (2017) 842.6–842.6.

[108]. Braun DJ, Bachstetter AD, Sudduth TL, Wilcock DM, Watterson DM, Van Eldik LJ, Genetic knockout of myosin light chain kinase (MLCK210) prevents cerebral microhemorrhages and

attenuates neuroinflammation in a mouse model of vascular cognitive impairment and dementia, Geroscience 41(5) (2019) 671–679. [PubMed: 31104189]

[109]. Berthiaume AA, Hartmann DA, Majesky MW, Bhat NR, Shih AY, Pericyte Structural Remodeling in Cerebrovascular Health and Homeostasis, Front Aging Neurosci 10(210) (2018) 210. [PubMed: 30065645]

[110]. Santos GSP, Magno LAV, Romano-Silva MA, Mintz A, Birbrair A, Pericyte Plasticity in the Brain, Neurosci Bull 35(3) (2019) 551–560. [PubMed: 30367336]

[111]. Allt G, Lawrenson JG, Pericytes: cell biology and pathology, Cells Tissues Organs 169(1) (2001) 1–11. [PubMed: 11340256]

[112]. Armulik A, Abramsson A, Betsholtz C, Endothelial/pericyte interactions, Circ Res 97(6) (2005) 512–23. [PubMed: 16166562]

[113]. Armulik A, Genove G, Mae M, Nisancioglu MH, Wallgard E, Niaudet C, He L, Norlin J, Lindblom P, Strittmatter K, Johansson BR, Betsholtz C, Pericytes regulate the blood-brain barrier, Nature 468(7323) (2010) 557–61. [PubMed: 20944627]

[114]. Azimi MS, Motherwell JM, Dutreil M, Fishel RL, Nice M, Hodges NA, Bunnell BA, Katz A, Murfee WL, A novel tissue culture model for evaluating the effect of aging on stem cell fate in adult microvascular networks, Geroscience 42(2) (2020) 515–526. [PubMed: 32206968]

Highlights

- Most rat cerebrovascular pericytes are α-SMA positive
- CYP4A and α-SMA coexpress in rat cerebral VSMCs and most pericytes
- 20-HETE is positively correlated with cerebral mural cell contractility
- 20-HETE promotes the myogenic response of rat parenchymal arterioles
- 20-HETE enhances CBF autoregulation in rat surface and deep cortex

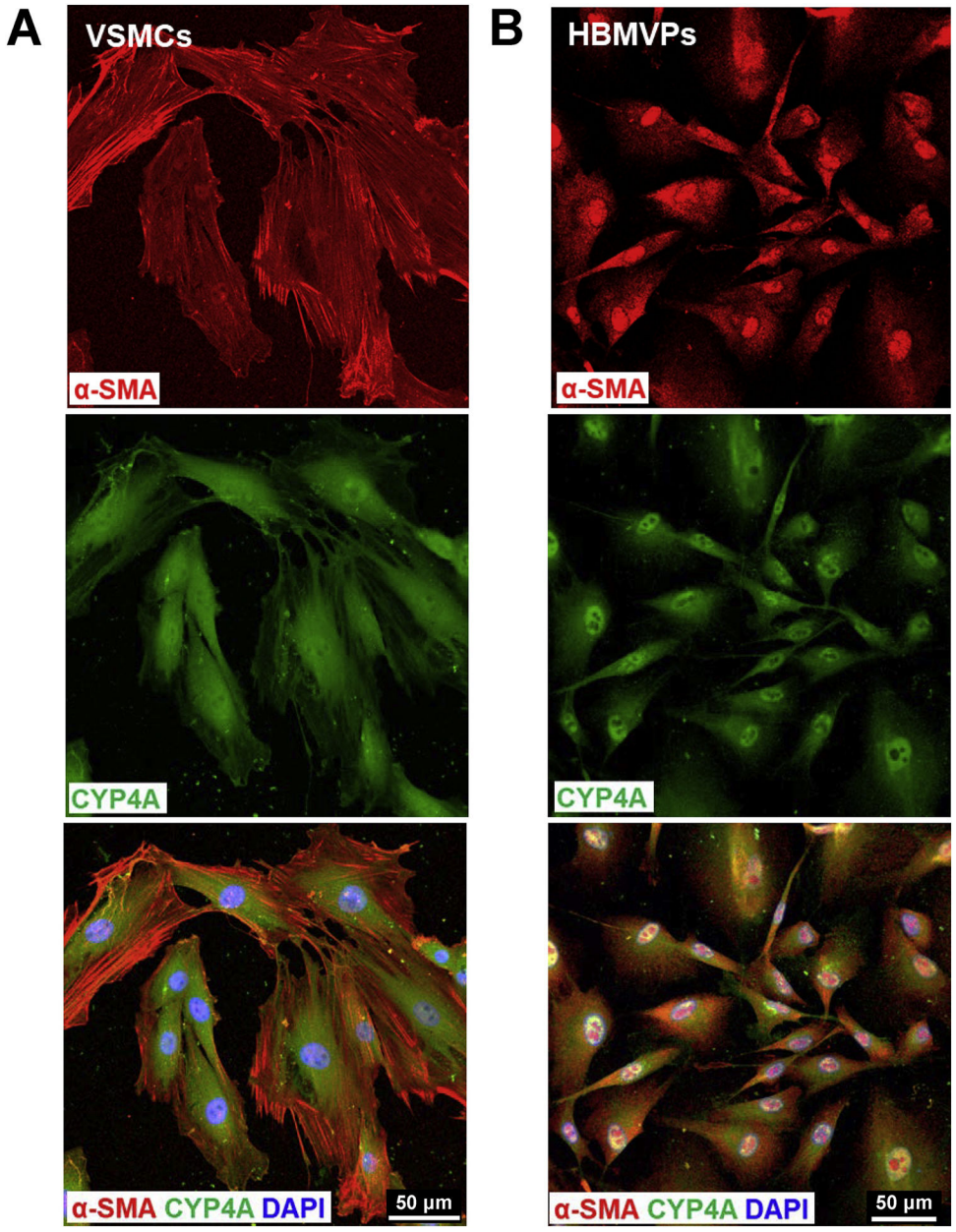

Figure 1. CYP4A is expressed in rat cerebral VSMCs and pericytes that express α-SMA

A: Representative images of the expression of CYP4A and α-SMA in primary cerebral VSMCs isolated from the MCA of SD rats. **B:** Representative images of the expression of CYP4A and α-SMA in the HBMVPs. The slides were imaged with a Nikon C2+ confocal head mounted on an Eclipse Ti2 inverted microscope (Nikon) using a 20 X objective and 2 X digital zoom (total magnification of 880 X). VSMCs, vascular smooth muscle cells; α-SMA, alpha-smooth muscle actin; MCA, middle cerebral artery; SD, Sprague Dawley; HBMVPs, human brain microvascular pericytes.

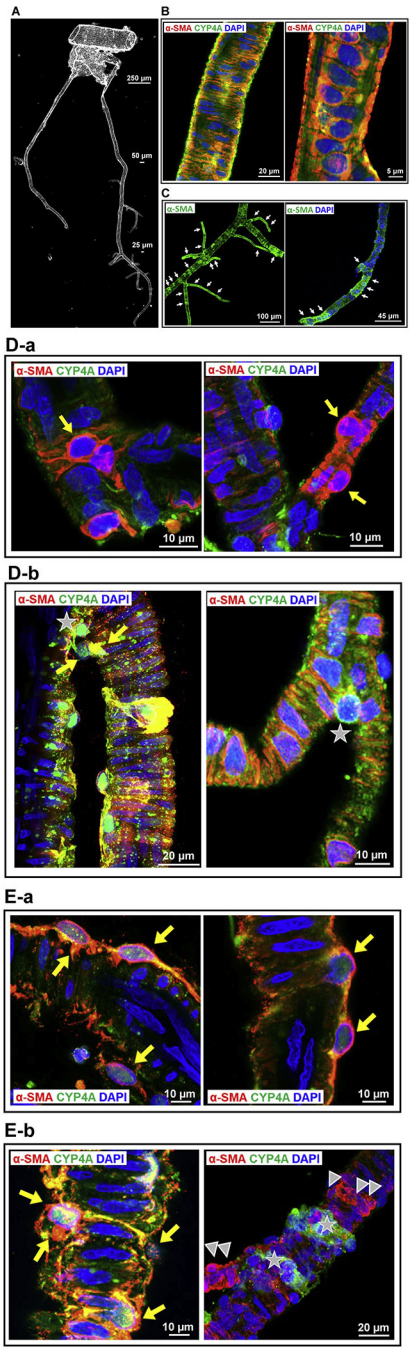

Figure 2. CYP4A expression pattern in cerebral VSMCs and pericytes on the vessel wall in the MCA territory in isolated rat cerebral vasculature

A: Representative phase-contrast image of the vascular structure and organization of isolated vessels from SD rats in the MCA territory. **B:** Representative images of the expression of CYP4A and α-SMA in VSMCs in the arterioles. **C:** The expression of α-SMA was detected in mural cells in the arterioles and capillaries in isolated rat cerebral vasculature without a clear defined terminus. **D:** Representative images of the expression of CYP4A and α-SMA in ensheathing or mesh pericytes on the sidewall (a) and junctions of the arterioles and

capillaries (b; video 1, 2). **E:** Representative images of the expression of CYP4A and α-SMA in thin-strand pericytes longitudinal along with the sidewall (a) and wrapping around the arterioles and capillaries (b; video 3). Arrows (white) indicate α-SMA expressed vascular areas (C). Arrows (yellow) indicate CYP4A and α-SMA coexpressed pericytes (D, E). Arrow-heads indicate α-SMA positive but CYP4A negative expressed pericytes. Pentagrams indicate α-SMA negative but CYP4A positive expressed pericyte (D-b) or cell clusters (E-b). Vessel sizes are indicated with size bars. VSMCs, vascular smooth muscle cells; MCA, middle cerebral artery; SD, Sprague Dawley; α-SMA, alpha-smooth muscle actin.

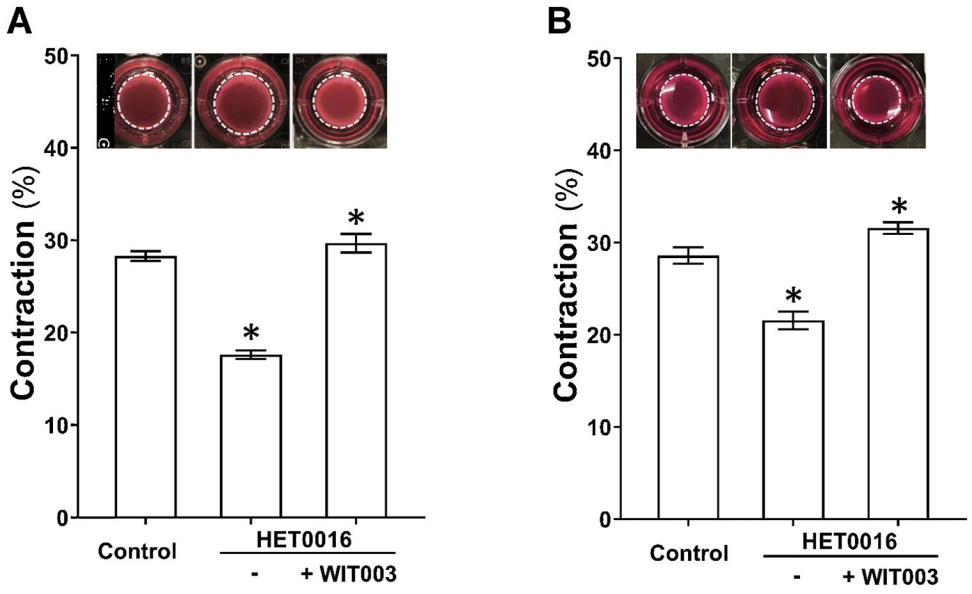

Figure 3. Impact of 20-HETE cerebral VSMCs and pericytes contractile capability

A: Comparison of the contractile capability of primary VSMCs isolated from the MCA of SD rat treated with HET0016 in the absence or presence of WIT003. **B:** Comparison of the contractile capability of HBMVPs treated with HET0016 in the absence or presence of WIT003. The inserts are representative images and the white dotted circles represent the gel area after stimulation. Experiments were repeated 3–4 times in triplicates. * indicates $P < 0.05$ from the corresponding values in drugs-treated cells versus controls. VSMCs, vascular smooth muscle cells; MCA, middle cerebral artery; SD, Sprague Dawley; HET0016, N-Hydroxy-N′-(4-butyl-2-methylphenyl)-formamidine; WIT003, 20-hydroxyeicosa-5(Z),14(Z)-dienoic acid; HBMVPs, human brain microvascular pericytes.

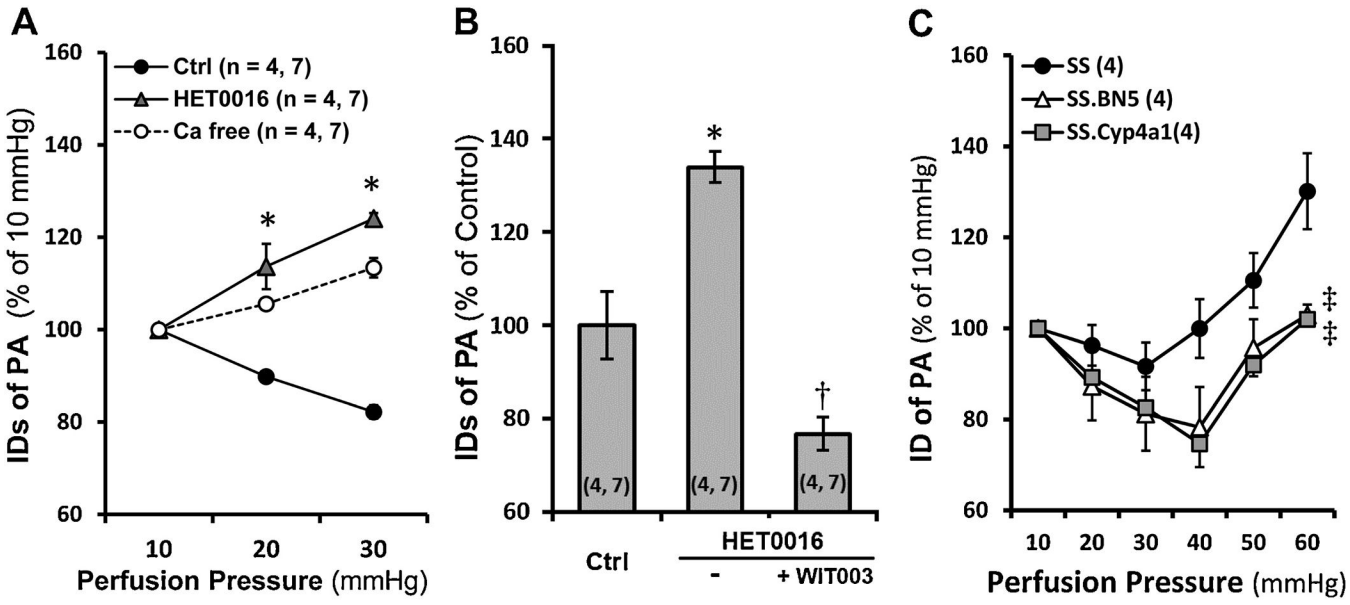

Figure 4. Impact of 20-HETE on the myogenic response of isolated rat Pas

A: Comparison of the luminal diameters of the PAs isolated from SD rats in response to increased perfusion pressure with or without HET0016 treatment. Passive diameters were recorded in calcium-free solution. **B:** Comparison of changes in luminal diameters of the PAs isolated from SD rats in response to HET0016 in the absence or presence of WIT003. **C:** Comparison of changes in luminal diameters of PAs isolated from SS, SS.BN5, and SS.*Cyp4a1* rats. Mean values ± SEM are presented. Numbers in parentheses indicate the number of animals and vessels studied. * indicates $P < 0.05$ from the corresponding values in control group. † indicates $P < 0.05$ from the corresponding values of HET0016-treated PAs in the absence or presence of WIT003. ‡ indicates $P < 0.05$ from the corresponding values of SS rats. PAs, parenchymal arterioles; SD, Sprague Dawley; SS, Dahl salt-sensitive rats; HET0016, N-Hydroxy-N′-(4-butyl-2-methylphenyl)-formamidine; WIT003, 20-hydroxyeicosa-5(Z),14(Z)-dienoic acid.

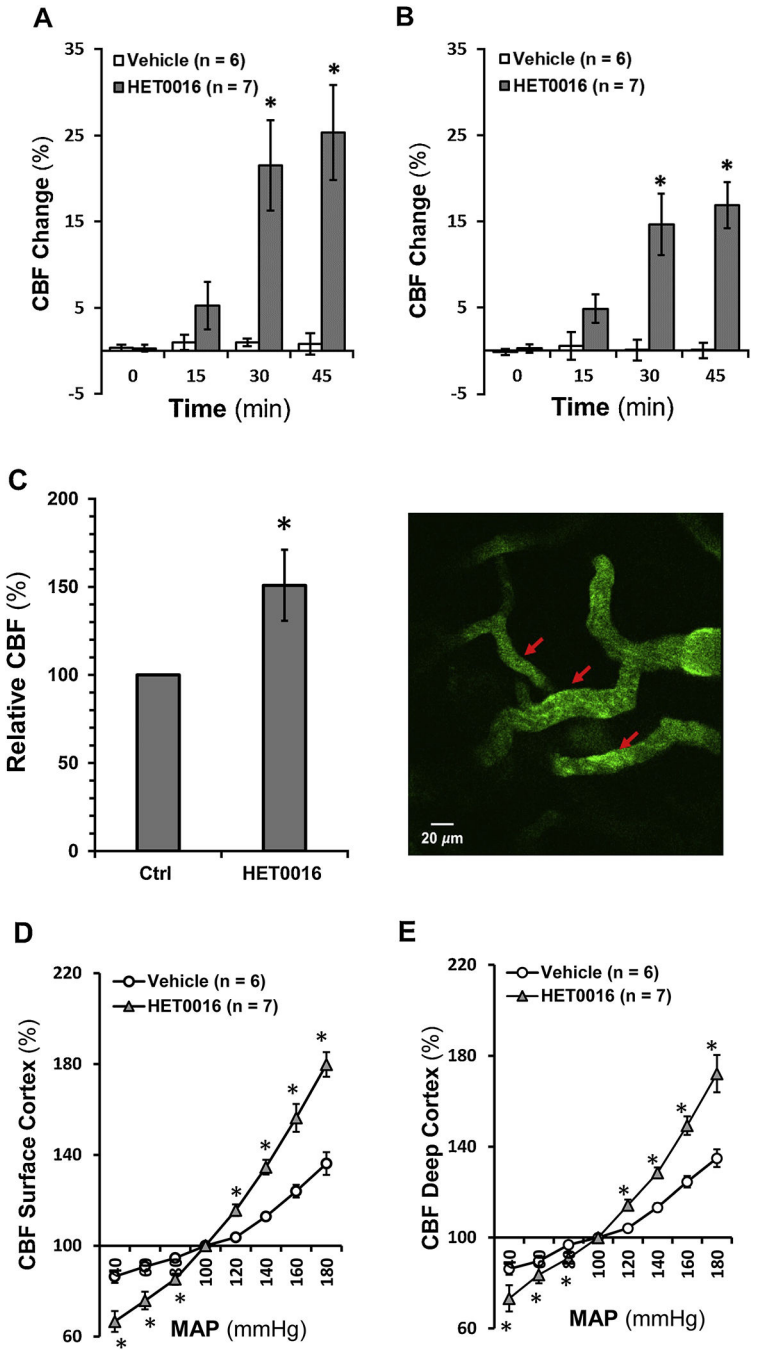

Figure 5. Impact of 20-HETE on CBF autoregulation in rat superficial and deep cortex

A: Comparison of rat surface cortical CBF changes in response to HET0016 with time. **B:** Comparison of rat deep cortical CBF changes in response to HET0016 with time. **C:** Left: Comparison of relative CBF, estimated by RBC velocities of cortical microvessels in response to HET0016 using TPLSM in SD rats. Right: a reparative image of cortical cerebral microvessels and the sight of RBC velocities measurements (red arrows). **D:** Comparison of CBF autoregulation in rat superficial cortex. **E:** Comparison of CBF autoregulation in rat deep cortex. Mean values ± SEM are presented. Numbers in

parentheses indicate the number of animals studied. * indicates $P < 0.05$ from the corresponding values in HET0016-treated versus -untreated rats. CBF, cerebral blood flow; TPLSM, two-photon laser-scanning microscopy; RBC, red blood cell; HET0016, N-Hydroxy-N′-(4-butyl-2-methylphenyl)-formamidine; SD, Sprague Dawley.